Route to Drift Wave Chaos and Turbulence in a Bounded Low- β Plasma Experiment

T. Klinger, A. Latten, A. Piel, Gildas Bonhomme, Th. Luc Pierre, Thierry Dudok de Wit

Route to Drift Wave Chaos and Turbulence in a Bounded Low-β Plasma Experiment

T. Klinger,[1] A. Latten,[1] A. Piel,[1] G. Bonhomme,[2] T. Pierre,[2] and T. Dudok de Wit[3]
[1]*Institut für Experimentalphysik, Christian-Albrechts-Universität, D-24098 Kiel, Germany*
[2]*Laboratoire de Physique des Milieux Ionisés, Université Henri Poincaré, F-54506 Vandœuvre-lès-Nancy, France*
[3]*CNRS Centre de Physique Théorique, Luminy, F-13288 Marseille, France*
(Received 6 June 1997)

The transition scenario from stability to drift wave turbulence is experimentally investigated in a magnetized low-β plasma with cylindrical geometry. It is demonstrated that the temporal dynamics is determined by the interaction and destabilization of spatiotemporal patterns, in particular, traveling waves. The analysis of the temporal and the spatiotemporal data shows that the bifurcations sequence towards weakly developed turbulence follows the Ruelle-Takens scenario. [S0031-9007(97)04530-4]

PACS numbers: 52.35.Kt, 05.45.+b, 52.35.Ra

It is an essential feature of bounded plasmas to establish edge localized gradients in the density, the space charge potential, and the particle temperatures. The magnetized plasma is then subjected to a class of low-frequency electrostatic fluid drift instabilities, the collisional drift waves. The dynamics of collisional drift waves is based on the tight coupling of fluctuations caused by $\boldsymbol{E} \times \boldsymbol{B}$ and diamagnetic drifts perpendicular to the magnetic field and a resistive parallel electron response. Linear drift waves travel predominantly in the transverse direction with electron diamagnetic drift velocity, have a radial eigenmode structure, and tend to establish axially standing modes. Despite important recent progress in theory [1] and experiment [2], the nature of the drift wave turbulence is still far from being understood. In particular, little is known of the strongly nonlinear regime in between the linear instability onset and the fully developed turbulence. In this paper, we describe an experimental study of the transition from a stable state to weakly developed drift wave turbulence in a bounded cylindrical low-β plasma. When the control parameter is increased, the transition follows a well-defined scenario, analogously to the already classical observations in neutral fluids [3]. Of high general interest in spatially extended, dissipative systems is the relationship between the temporal dynamics and spatiotemporal patterns [4], for instance, traveling waves, and we thus devote special attention to this important subject.

The drift wave experiment was performed in a triple plasma device with a magnetized central chamber [5]. In one chamber a thermionic argon discharge is operated as plasma source (gas pressure $P = 8 \times 10^{-4}$ mbar). The weakly ionized plasma diffuses into the central section and forms a magnetized column (magnetic field $B = 70$ mT) of length $l = 1.6$ m with a Gaussian radial density profile $n(r) = n_0 \exp(-r^2/2r_0^2)$ of width $r_0 = 2.0$ cm. The plasma column is bounded on both ends by transparent grids separating it from the source chambers. In the center of the column the electron temperature is $T_e = 1.2$ eV and the electron density is $n_e = 2 \times 10^{16}$ m^{-3}. From laser diagnostics in thermionic discharges an ion temperature close to gas temperature was inferred [6], i.e., $T_e/T_i \approx 40$. The drift wave characteristic length scales are set by the reduced gyroradius $\rho_s = 1.0$ cm and the inverse density gradient length $L_n^{-1} = d(\ln n)/dr = 1/r = 0.5$ cm^{-1} [7]. The time scale is given by the drift wave frequency $\omega^* = (k_b T_e/eB) L_n^{-1}/r = 4.3 \times 10^4$ rad/s [7] which is below the ion cyclotron frequency $\omega_{ci} = 1.7 \times 10^5$ rad/s. It is shown below that part of the fluctuation spectra may well exceed ω_{ci} and the low-frequency approximation starts to fail.

We now identify the control parameter that determines the drift wave stability properties. It was shown previously [8] that a positively biased separation grid gives rise to a static radial electric field E_r in the magnetized plasma column. The resulting $E_r \times B$ rotation strongly destabilizes collisional drift waves, mainly due to centrifugal forces acting on the ion fluid [2,8]. In our experiment, emissive probe measurements have revealed a sheath structure at the grid establishing a parabolic radial potential profile. The shearless $E_r \times \boldsymbol{B}$ rotation of the plasma column is then determined by the grid bias and for $U_g = 0$–8 V (well below the argon ionization potential) we find a monotonous increase of the angular velocity of the column in the range $\omega_{\boldsymbol{E}\times\boldsymbol{B}} = B^{-1} d\phi_p/dr = (2$–$6) \times 10^4$ rad/s (of the same order as ω^*). This makes U_g a suitable external parameter that controls the plasma rotation and thus the stability properties (thereby the dynamical state) of rotation-induced collisional drift waves.

Biased Langmuir probes located at the radial position r_0 of the maximum density gradient are used for the measurement of density fluctuations to investigate the temporal and the spatiotemporal drift wave dynamics. For the latter, a novel diagnostic tool was developed [5], a circular probe array consisting of 64 probes. The probe array data has a temporal resolution $\Delta t \geq 1$ μs and a spatial resolution of 0.4 cm. In cylindrical geometry, the azimuthal boundary conditions are periodic and the drift waves are restricted to integer azimuthal mode numbers m. The Nyquist limit of the probe array is then $m_{\mathrm{Nyq}} = 32$.

We first restrict the discussion to the temporal dynamics of drift waves. In Fig. 1, for increasing control parameter, time series of a single negatively biased probe, its power spectrum, and the phase space diagram are shown. The phase space reconstruction is made by delay time embedding [9] with parameters d (embedding dimension) and τ (delay time) determined by the so-called fill factor criterion [9]. The normalized control parameter is defined by $\epsilon = (U_g - U_{gc})/U_{gc}$, where $U_{gc} = 3.5$ V is the (critical) grid bias of the onset of the drift instability. The transition scenario to chaos and turbulence is observed as follows. The first Hopf bifurcation occurs at the linear instability onset of a drift mode at $\epsilon = 0.0$. The drift mode saturates by generating higher harmonics as shown in Fig. 1(a) for $\epsilon = 0.14$. The phase space attractor is a limit cycle and the frequency power spectrum is sharply peaked at the mode frequency $f_3 = 13.5$ kHz (Doppler shifted by $f_{E\times B} \approx 3.0$ kHz) and its higher harmonics which are close or in excess of the ion cyclotron frequency. The next Hopf bifurcation at $\epsilon = 0.33$ introduces a second drift mode with frequency $f_1 = 6.9$ kHz [Fig. 1(b), note the increased Doppler shift]. This mode is nonlinearly unstable and is the result of the nonlinear saturation [10] of the previously excited mode at $f_3 = 18.8$ kHz. Because of the parametric interaction of the two waves [10] with incommensurate frequencies, the power spectrum is multipeaked at sum and difference of integer multiples of the two mode frequencies $f_{ij} = if_3 \pm jf_1$ with $i, j \in \mathbb{N}$, where each frequency f_{ij} corresponds to an originally damped daughter wave. The phase space attractor of such a quasiperiodic state is a two-torus and the time series shows no periodicity [Fig. 1(b)]. The subsequent bifurcation to mode locking [11] happens at $\epsilon = 0.56$ [Fig. 1(c)]. In comparison to the quasiperiodic state the frequency power spectrum is greatly simplified. There are only two strong peaks (and higher harmonics) left at $f_1 = 7.9$ kHz and $f_2 = 15.8$ kHz $= 2f_1$, where the higher frequency peak is the stronger one. Such a subharmonic spectrum is a hallmark of higher periodic behavior, as apparent from the double loop phase space attractor and the time series with a strict periodicity two. A further increase of the control parameter leads to the gradual dissolution of the mode-locked state [Fig. 1(d)]. Inspecting the time series, it is found that the periodicity of the series experiences a slow evolution until it is occasionally interrupted (at $t \approx 0.9$ ms) in Fig. 1(d). This means that the periodic orbit shown in Fig. 1(c) has become unstable [12] and the excursions to irregular behavior broaden the spectrum, increase the noise level, and fill up previously empty regions of the phase space attractor. A further increase of the control parameter leads to strongly irregular behavior [Fig. 1(e)] and finally to turbulence [Fig. 1(f)] with a broad, noiselike frequency power spectrum, intermittent fluctuations, and a scattered phase space distribution. During the transition to turbulence the maximum relative

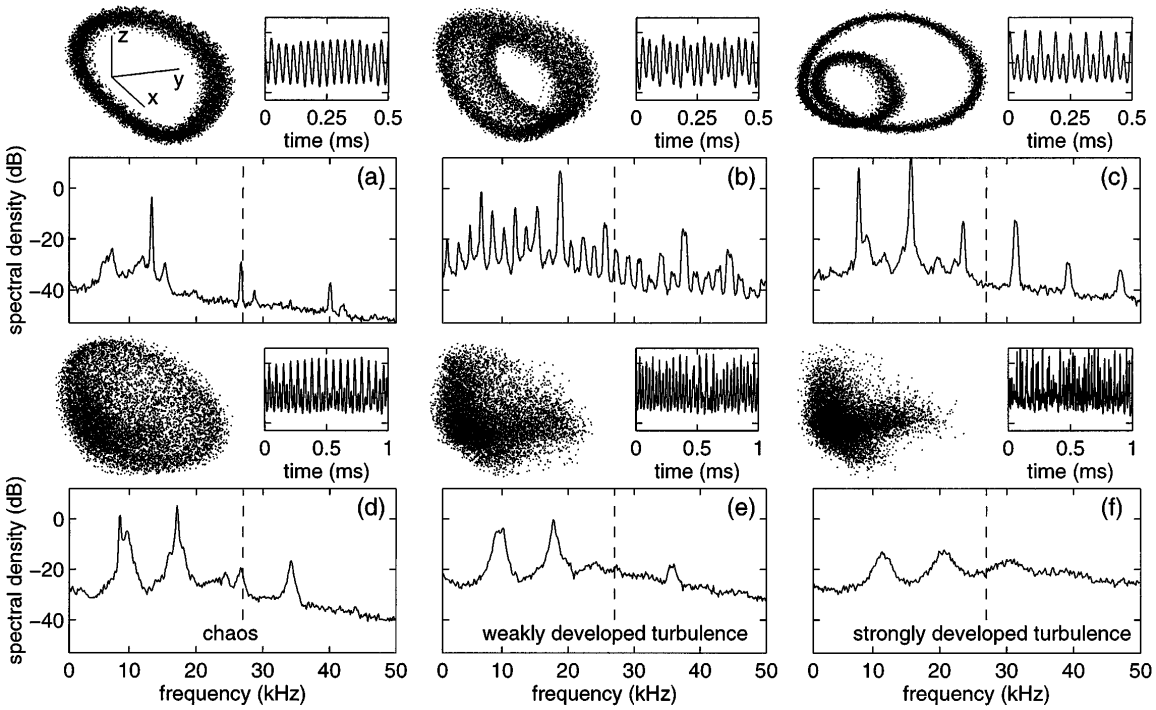

FIG. 1. Temporal dynamics of the transition to weakly developed turbulence. In each subfigure, the time series of density fluctuations, its power spectrum (the dashed line indicates the ion cyclotron frequency ω_{ci}), and the phase space contour are shown (delay time embedding in here $d = 3$ dimensions with $\{X, Y, Z\} = \{n(t), n(t + \tau), n(t + 2\tau)\}$ where τ varies between 9–11 samples). The control parameter values are (a) $\epsilon = 0.14$, (b) $\epsilon = 0.50$, (c) $\epsilon = 0.57$, (d) $\epsilon = 0.74$, (e) $\epsilon = 0.86$, and (f) $\epsilon = 0.93$.

density fluctuation level increases from $\tilde{n}/n < 10\%$ up to 50%, the latter indicating strong turbulence. At this point, it is already reasonable to suggest the above described chain of events as being the classical Ruelle-Takens route to turbulence [3] previously observed in theoretical drift wave studies, too [13].

The spatiotemporal dynamics of the transition to turbulence is shown in Fig. 2. Spatiotemporal patterns of the density fluctuations $n(x,t)$ are shown for increasing control parameter together with the frequency-wave number (full) spectra estimated by discrete Fourier transform of $n(x,t)$ (it is $x \in [0, 2\pi]$ and $t \in [0, T]$ with $n(0,t) = n(2\pi,t)$ and $N = T/\Delta t \gg 1$). After the first Hopf bifurcation, the $n(x,t)$ diagram is periodic and shows a coherent traveling wave with mode number $m = 3$ and a frequency $f_3 = 19$ kHz [Fig. 2(a)]. The spatiotemporal pattern $n(x,t)$ becomes quasiperiodic after the second Hopf bifurcation [Fig. 2(b)]. Here an additional $m = 1$ mode with a frequency $f_1 = 7.1$ kHz (incommensurate to f_3) is in nonresonant three-wave interaction with the $m = 3$ mode. This is clearly seen in the power spectrum of the quasiperiodic state where, besides the fundamental $m = 1$ and $m = 3$ modes, a whole set of forced daughter waves is found (most pronounced $m = 2$ but also $m = 4$ and $m = 5$ due to nonlinear interaction of the higher harmonics). The bifurcation from the quasiperiodic to the mode-locked state is a transition from nonresonant interaction of the $m = 1$ and $m = 3$ modes to the resonant interaction of the $m = 1$ and $m = 2$ modes, initiated by an eventual resonance overlap of forced $m = 2$ modes. The spatiotemporal pattern $n(x,t)$ is two periodic in space and time [Fig. 2(c)] and in the spectrum a strong peak occurs at $m = 2$ and a weaker one at $m = 1$. The other spectral components are just higher harmonics in frequency and wave number, as required for resonant coupling. This two-periodic spatiotemporal pattern is remarkably stable. It needs a significant increase of the control parameter to destabilize the structure as shown in Fig. 2(d). Occasionally the periodicity (and thereby the spatiotemporal symmetry) of $n(x,t)$ is broken by small phase dislocations, respectively, defects [4] [in Fig. 2(d) emphasized by a box]. These defects have a relatively short lifetime of the order of the period duration of the $m = 1$ mode and lead to the broadening of the spectrum around the two dominant peaks. The further increase of the control parameter results in the total loss of the spatiotemporal symmetry of $n(x,t)$ and a turbulent state is established [Fig. 2(e)]. The resultant spectrum is broad banded in frequency and wave number.

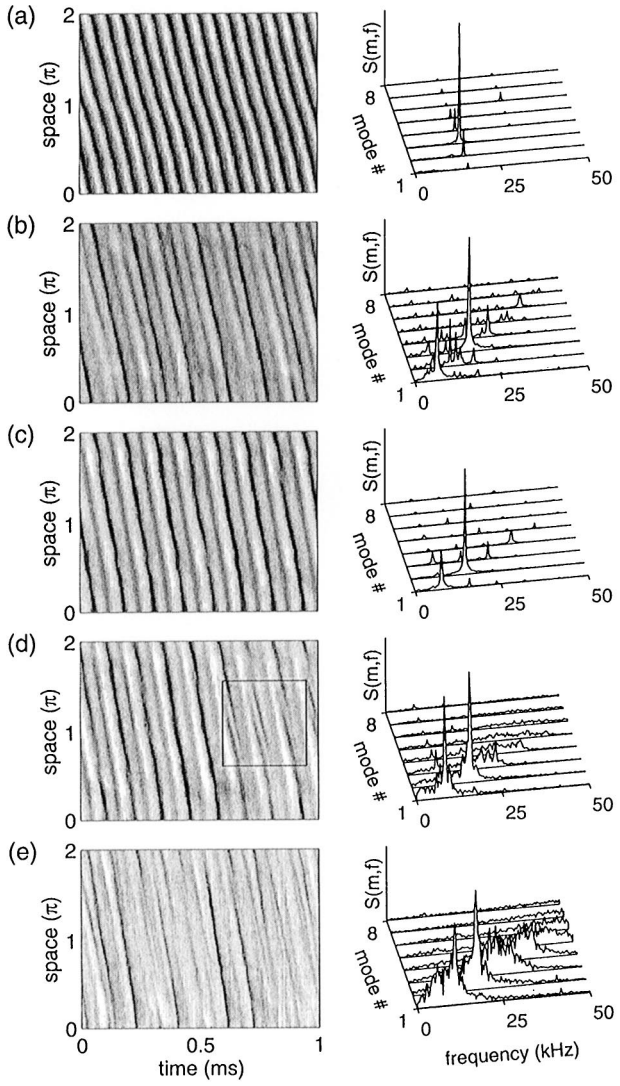

FIG. 2. Spatiotemporal dynamics of the transition scenario to weakly developed turbulence. Spatiotemporal density fluctuations (left, gray-scale coded) and power spectra (right). Control parameter values are (a) $\epsilon = 0.13$ (periodic), (b) $\epsilon = 0.49$ (quasiperiodic), (c) $\epsilon = 0.62$ (mode lock), (d) $\epsilon = 0.75$ (chaotic), and (e) $\epsilon = 1.01$ (weakly turbulent).

The most important ergodic phase space measures, i.e., the (correlation) dimension [14] and the spectrum of Lyapunov exponents [15], have been estimated. The result is shown in Figs. 3(b) and 3(c). At each Hopf-bifurcation point the attractor dimensionality increases by one indicating an additional degree of freedom (equivalent to additional drift mode). The dimensionality is reduced by one during the transition from the quasiperiodic to the mode-locked state since the trajectories do no longer cover the surface of the torus but form a double loop [cf. Fig 1(c)]. The destabilization of the mode-locked state for $\epsilon_c > 0.7$ becomes apparent by a steep increase of the dimensionality that fits the scaling law $D_2(\epsilon) = D_2^{\mathrm{ml}} + \gamma(\epsilon - \epsilon_c)^{3/4}$, where $D_2^{\mathrm{ml}} = 1.1 \pm 0.1$ is the dimensionality of the mode-locked state. The Lyapunov spectrum Fig. 3(c) shows how the stability properties of the different attractors change. The limit cycle has a spectrum $(0, -, -)$ and the negative Lyapunov exponents decrease while the mode saturates, indicating a gain of stability. The second Hopf bifurcation changes the spectrum to $(0, 0, -)$ as required for a two-torus with an additional invariant direction in phase space. The bifurcation to the mode-locked state reestablishes the $(0, -, -)$ spectrum similar to that of the limit cycle. With the steep increase of the dimensionality

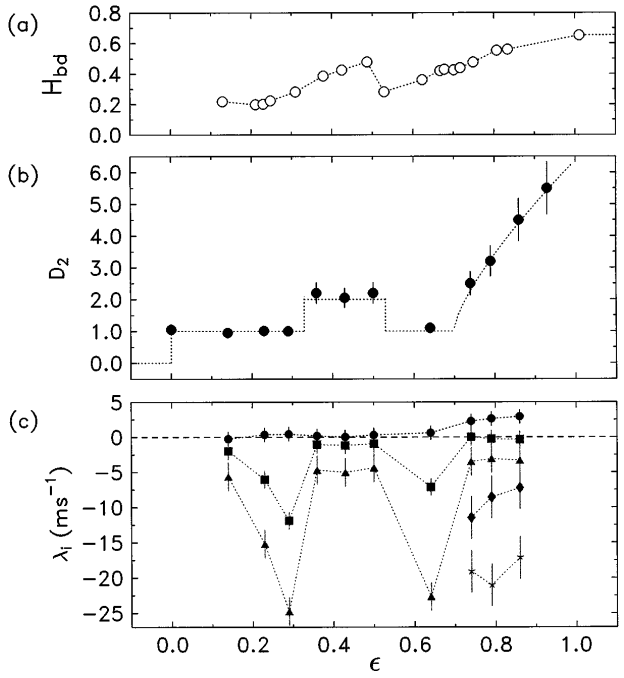

FIG. 3. (a) Biorthogonal global entropy H_{bd} of the data set Fig. 2. (b) Correlation dimension D_2 and (c) Lyapunov spectrum λ_i of the data set partially shown in Fig. 1. Lines are drawn to guide the eye.

a positive Lyapunov exponent arises indicating the loss of stability in phase space, i.e., chaotic behavior. The Lyapunov spectrum then has the structure $(+, 0, -, -, -)$ in the appropriately enlarged embedding space. The evolution of the dimensionality and the Lyapunov spectrum confirms quantitatively the Ruelle-Takens transition scenario.

We finally investigate the spatiotemporal dynamics by means of a linear technique called biorthogonal decomposition (BD), also known as proper orthogonal decomposition [16]. The wave field $n(x,t)$ is decomposed in a real weighted sum of purely spatial and temporal eigenmodes

$$n(x,t) = \sum_{k=1}^{N} a_k \phi_k(x) \psi_k(t) \qquad (1)$$

with $(\phi_k, \phi_l) = (\psi_k, \psi_l) = \delta_{kl}$ being the eigenmodes of the two-point spatial and temporal correlation functions. In case of degeneracy $a_k = a_{k+1}$ they are identical to traveling waves [16]. In a complementary investigation [17] the BD already proved being a powerful data analysis instrument suggesting a set of differential equations that describe the nonlinear coupling and the destabilization of waves. In Refs. [16] an entropy-type measure of the spatiotemporal complexity was introduced:

$$H_{\mathrm{bd}} = -\frac{1}{\ln N} \sum_{k=1}^{N} p_k \ln p_k \in [0,1], \qquad (2)$$

where $p_k = a_k^2 / \sum_n a_n^2 \in [0,1]$ are the normalized squared weights. In Fig. 3(a) the dependence of H_{bd} of the control parameter ϵ is shown. For both a single mode and the mode-locked state $H_{\mathrm{bd}} \approx 0.2$ while the global entropy indicates increasing spatiotemporal complexity after the second Hopf bifurcation, where a large number of daughter waves are driven by the nonresonant interaction of two modes. The destabilization of the mode-locked state and the transition to spatiotemporal chaos becomes apparent by a steady increase of H_{bd} for $\epsilon > 0.53$, meaning increasing spatiotemporal disorder. We note that the BD as a *linear* spatiotemporal analysis tool yields results that qualitatively agree with the ergodic measures of the *nonlinear* phase space description.

To summarize, the drift wave experiments in an axially bounded rotating low-β plasma column reveal an *a priori* unexpected similarity to Rayleigh-Bénard convection cell experiments [18]. The transition to chaos and turbulence follows clearly the Ruelle-Takens scenario and the destabilization of the mode-locked state is related to the occurrence of defects in the spatiotemporal pattern. Fully developed turbulence means strong spatiotemporal disorder. The analysis of the ergodic phase space measures and the global biorthogonal entropy reveals the entanglement of the temporal and the spatiotemporal dynamics.

This work was supported by the Deutsche Forschungsgemeinschaft Grant No. Pi 185/6–1/2.

[1] D. Biskamp and A. Zeiler, Phys. Rev. Lett. **74**, 706 (1995); B. Scott, Plasma Phys. Controlled Fusion **39**, 471 (1997).
[2] H. L. Pécseli, T. Mikkelsen, and S. E. Larsen, Plasma Phys. Controlled Fusion **25**, 1173 (1983).
[3] P. Manneville, *Dissipative Structures and Weak Turbulence* (Academic Press, San Diego, 1990).
[4] M. C. Cross and P. C. Hohenberg, Rev. Mod. Phys. **65**, 851 (1993).
[5] A. Latten *et al.*, Rev. Sci. Instrum. **66**, 3254 (1995).
[6] G. Bachet *et al.*, Phys. Fluids B **5**, 3097 (1993).
[7] Taken at the maximum density gradient position r_0.
[8] E. Marden Marshall, R. F. Ellis, and J. E. Walsh, Plasma Phys. Controlled Fusion **28**, 1461 (1986).
[9] T. Buzug and G. Pfister, Physica (Amsterdam) **58D**, 127 (1992).
[10] F. Hai and A. Y. Wong, Phys. Fluids **13**, 672 (1970).
[11] J. A. Glazier and A. Libchaber, IEEE Trans. Circuits Syst. **35**, 790 (1988).
[12] C. Grebogi, E. Ott, and J. A. Yorke, Phys. Rev. A **37**, 1711 (1988).
[13] D. Biskamp and K. F. He, Phys. Fluids **28**, 2172 (1985); T. Eickermann and K. H. Spatschek, Phys. Rev. E **51**, 1605 (1995).
[14] P. Grassberger and I. Procaccia, Phys. Rev. Lett. **50**, 346 (1983).
[15] T.-M. Kruel, M. Eiswirth, and F. W. Schneider, Physica (Amsterdam) **63D**, 117 (1993).
[16] N. Aubry, R. Guyonnet, and R. Lima, J. Stat. Phys. **64**, 683 (1991); J. Nonlinear Sci. **2**, 183 (1992); P. J. Holmes *et al.*, Phys. Rep. **287**, 337 (1997).
[17] A. Madon and T. Klinger, Physica (Amsterdam) **91D**, 301 (1996); **102D**, 335 (1997).
[18] S. W. Morris *et al.*, Phys. Rev. Lett. **71**, 2026 (1993); A. La Porta and C. M. Surko, Phys. Rev. Lett. **77**, 2678 (1996).